ACCSCIENCE PUBLISHING

Innovative Medicines & Omics

ORIGINAL RESEARCH ARTICLE

Lactylation-orchestrated Tprolif dynamics in skin cutaneous melanoma: Prognostic significance and therapeutic implications

Qianyu Shen†, Sirui Qian†, Yanan Yan, Xinhan Wu, Yingjia Ni, Maorong Suo*, and Yuan Wu*

Department of Biology and Environment, College of Jiyang, Zhejiang A&F University, Hangzhou, Zhejiang, China

Abstract

Skin cutaneous melanoma is a highly aggressive malignancy with poor prognosis, particularly in advanced stages. Lactylation, a post-translational modification, plays a crucial role in shaping the tumor microenvironment and contributing to immune suppression, making it a potential therapeutic target. In this study, single-cell RNA sequencing data from the Tumor Immune Single-cell Hub database and bulk RNA sequencing data from The Cancer Genome Atlas and Gene Expression Omnibus were analyzed. Lactylation-related genes were obtained from the Molecular Signatures Database, and lactylation scores for each cell type were computed using the AUCell R package. Cell–cell communication networks were constructed using CellChat, and a prognostic model was developed based on machine learning—including least absolute shrinkage and selection operator, random forest, and XGBoost. Drug candidates were identified via the L1000 Fireworks Display database and the Comparative Toxicogenomics Database, followed by molecular docking for drug–target interaction assessment. Results revealed that Tprolif cells exhibited the highest lactylation levels, indicating their immunosuppressive role in the tumor microenvironment, with the macrophage migration inhibitory factor receptor–ligand pathway identified as a key interaction hub. The eight lactylation-related genes–Tprolif prognostic model demonstrated moderate predictive ability for patient survival, and BG-FA-0953 emerged as a potential therapeutic candidate that may target lactylation-related pathways, warranting further investigation. This study provides novel insights into lactylation-driven immune modulation in skin cutaneous melanoma, with potential implications for risk stratification and therapeutic intervention in advanced-stage melanoma.

Keywords: Skin cutaneous melanoma; Lactylation; Tumor microenvironment; Machine learning; Prognosis; Therapeutic targets

†*These authors contributed equally to this work.*

***Corresponding authors:**
Maorong Suo
(suomaorong@163.com);
Yuan Wu
(yuanwu@zjyc.edu.cn)

Citation: Shen Q, Qian S, Yan Y, *et al*. Lactylation-orchestrated Tprolif dynamics in skin cutaneous melanoma: Prognostic significance and therapeutic implications. *Innov Med Omics*. 2026;3(4):026200023. doi: 10.36922/IMO026200023

Received: May 11, 2026

Revised: June 2, 2026

Accepted: June 9, 2026

Published online: July 7, 2026

Copyright: © 2026 Author(s). This is an Open-Access article distributed under the terms of the Creative Commons Attribution License, permitting distribution, and reproduction in any medium, provided the original work is properly cited.

Publisher's Note: AccScience Publishing remains neutral with regard to jurisdictional claims in published maps and institutional affiliations.

1. Introduction

Skin cutaneous melanoma (SKCM) is one of the most prevalent and aggressive malignancies globally, with a notably higher incidence in Caucasian populations.[1] It originates from melanocytes, which are pigment-producing cells within the epidermis derived from the neural crest.[2] Ultraviolet radiation is the most important risk factor

for SKCM, while rare subtypes are not correlated with ultraviolet radiation exposure.[3] Despite SKCM representing merely 4% of all skin cancer cases, it accounts for 75% of skin cancer-related deaths, and is characterized by its propensity for rapid metastasis to distant organs, resulting in significantly poor clinical outcomes.[4] Early-stage SKCMs generally exhibit favorable prognostic outcomes—over 90% of SKCMs are cured with early detection and proper treatment[5]; however, thick primary tumors and metastatic SKCM still have high mortality rates.[6]

Over the past decades, immunotherapy such as immune-checkpoint inhibitors and targeted therapies like BRAF inhibitors have revolutionized the treatment regimen of melanoma. Nevertheless, the five-year survival rate of patients with advanced-stage SKCM is still at most 50%.[7] In recent years, novel therapeutic strategies—such as tumor-infiltrating lymphocytes—have emerged; however, they are not widely available due to their complex nature and the need for highly specialized medical infrastructure.[8] Thus, it is essential to identify prognostic biomarkers for advanced-stage SKCM. In addition, more therapeutic agents should be discovered for monotherapy or combination therapy of advanced-stage SKCM.

Currently, immunotherapy is one of the major treatment strategies for advanced-stage SKCM, while 40–65% of programmed cell death protein 1-based treatments in SKCM fail due to immune escape[9], whereby a less immunogenic phenotype is acquired by cancer cells and they can suppress anti-tumor immune cells in the tumor microenvironment (TME).[10,11] In recent years, benefiting from advancements in biotechnology, particularly the application of single-cell sequencing and spatial transcriptomics, numerous studies have been dedicated to elucidating the complexity of the TME. For example, Durante *et al.*[12] revealed the complex TME of uveal melanoma based on single-cell RNA sequencing and identified *LAG3* as a potential immune checkpoint target for high-risk patients. Moreover, key immune and molecular features in metastatic melanoma were identified by Quek *et al.*[13], revealing an "immune-striving" TME and highlighting B cell signatures and specific melanoma subclones as potential therapeutic targets via multimodal single-cell analysis. Although significant progress has been made in the study of TME in cutaneous melanoma[14], a comprehensive understanding of the TME remains challenging, and more work is required to elucidate the TME of SKCM for optimization of personalized immunotherapy and cancer treatment strategies.

Recently, lactylation in the TME has emerged as an important area of research in cancer immunology and cellular metabolism, despite uncertainty regarding lactylation's role in tumorigenesis—whether as a minor regulator or a major driver.[15,16] Lactylation is a type of post-translational modification of proteins, which can be identified using peptide immunoprecipitation combined with high-sensitivity high-performance liquid chromatography–tandem mass spectrometry analysis.[17] Several reports indicate that lactylation in the TME is fundamental to the establishment of an immunosuppressive environment[18,19], and refer to lactylation as a potential target in cancer therapy.[20]

In this study, we performed a comprehensive single-cell analysis of lactylation patterns within the TME of SKCM, marking the first systematic investigation of lactylation across immune cell subsets. Our findings firstly identified Tprolif cells as the immune subtype with the highest lactylation level, highlighting their potential involvement in shaping the immunosuppressive TME. Cell communication analysis identified the macrophage migration inhibitory factor (MIF) receptor–ligand pathway as the most significant pathway between Tprolif cells and other cell types. Leveraging multiple machine learning algorithms, we developed a robust prognostic model integrating eight lactylation-related genes (LRGs), which were differentially expressed in Tprolif cells, providing a novel framework for risk stratification in SKCM patients.

Based on the expression pattern of eight LRGs, we identified BG-FA-0953 as a promising small-molecule therapeutic candidate targeting lactylation-related pathways, and also selected other potential candidate drugs through a gene–chemical network for potential combination therapy of SKCM. Collectively, our study offers critical insights into lactylation-driven immune modulation, presenting new avenues for prognostic evaluation and therapeutic intervention in melanoma.

2. Methodology

2.1. Data acquisition

Single-cell RNA sequencing (scRNA-seq) GSE123139 dataset for SKCM was acquired from The Tumor Immune Single Cell Hub 2.[21] The training cohort was The Cancer Genome Atlas (TCGA) SKCM dataset, which included RNA expression profiles of 435 patients with SKCM obtained from the TCGA database (https://portal.gdc.cancer.gov/).

The validation set was derived from GSE65904 database, which comprised 210 SKCM samples (http://www.ncbi.nlm.nih.gov/geo). A total of 294 LRGs were obtained from the MSigDB database (Table S1) (https://www.gsea-msigdb.org/gsea/msigdb).[22] In the TCGA dataset, TPM values were first subjected to a $\log2(x + 1)$ transformation.

Subsequently, to ensure comparability across datasets, both the TCGA and Gene Expression Omnibus expression matrices were processed using z-score normalization, where each gene's expression value was subtracted by its mean and divided by its standard deviation (Figure 1).

2.2. Single-cell RNA sequencing data processing and calculation of lactylation scores among cell types

The scRNA-seq data were analyzed using the R package Seurat (version 4.1.1, The Satija Lab, USA).[23] After normalization, highly variable genes were identified using FindVariableFeatures, and the top 2,000 features were selected. Principal component analysis (PCA) was performed to reduce dimensionality after gene expression in the dataset was standardized. Clustering was performed using the FindNeighbors function and FindClusters function at a suitable resolution of 0.7 (Figure S1). Based on the PCA results, uniform manifold approximation and projection (UMAP) was performed using the first 10 principal components, and a UMAP plot was generated.

Cell type information was incorporated into the "meta.data" of the Seurat object by assigning "Celltype..minor.lineage." Lactylation scores among cell types were assigned using the R package AUCell (https://bioconductor.org/packages/release/bioc/html/AUCell.html), which is used to assess lactylation gene set activity.

Plots of lactylation scores for different cell types were visualized by the R package ggplot2.[24] This score represents transcriptome-level gene set enrichment results, which indirectly infer potential protein lactylation status, rather than direct protein-level detection of lactylation modification. Differentially expressed genes (DEGs) for each cluster were identified using the FindAllMarkers function. Significant genes in DEGs of Tprolif cells with an absolute avg_$\log_2$FoldChange >1 and $p < 0.05$ were selected (Table S2).

2.3. Construction of cell–cell communication network

Intercellular communication networks were constructed and visualized using the R package CellChat (version 1.5.0, R Foundation, USA).[25] The CellChat database for humans, comprising 1,939 validated interactions, was utilized for the analysis. Downstream analysis involved inferring cell–cell communication probabilities using the functions "computeCommunProb" and "filterCommunication." Communication probabilities were assessed at both the signaling pathway and gene levels using the "computeCommunProbPathway" function. Significant ligand–receptor pairs and signaling pathways were visualized using multiple plot types, including circle plots, heatmaps, and chord plots.

2.4. Identification of lactylation-related genes and differentially expressed genes selection in TCGA-SKCM

For each cell, a lactylation score was calculated using AUCell. All cells in the scRNA-seq dataset were then divided into high- and low-lactylation groups using the global median AUCell score as the cutoff. Cells with scores above the median were assigned to the high-lactylation group, and those below the median were assigned to the low-lactylation group. Differential expression analysis between the high- and low-lactylation groups was performed using the Wilcoxon rank-sum test implemented in the FindAllMarkers function in Seurat. DEGs were selected based on $\log_2$FoldChange > 1 and adjusted p (Benjamini–Hochberg method) < 0.05. This yielded 954 DEGs (Table S3).

Moreover, Pearson's correlation analysis was performed to assess the relationship between the expression of each gene and lactylation scores, and the top 100 genes were selected (Table S4). There were 1,011 genes after the merging of the 954 DEGs and the top 100 lactylation-score–related genes, and they were named LRGs. The R package TCGAbiolinks[26] was used to download the expression and clinical data from the TCGA-SKCM project. Subsequently, differential expression analysis was performed using the R package limma[27] to compare gene expression differences between tumor and normal tissues. The design matrix was then constructed using the "model.matrix" function, followed by linear model fitting using the "lmFit" function. The "eBayes" function was applied for empirical Bayes methods to assess differential expression. Finally, the "topTable" function was used to filter DEGs based on criteria of $p < 0.05$ and absolute $\log_2$FoldChange) > 1, with further application of the Benjamini–Hochberg method for false discovery rate correction, setting an adjusted $p < 0.05$ as the final selection criterion (Table S5).

2.5. Kyoto Encyclopedia of Genes and Genomes and Gene Ontology pathway enrichment analysis

To identify biological pathways and functional categories associated with DEGs of Tprolif and LRGs, Gene Ontology (GO) and Kyoto Encyclopedia of Genes and Genomes (KEGG) enrichment analyses were performed using the R package clusterProfiler.[28] GO analysis categorizes genes into three main ontologies: biological process, cellular component, and molecular function. KEGG pathway analysis was employed to identify significantly enriched pathways in the DEGs of Tprolif and LRGs. The results of both GO and KEGG analyses were visualized using dot plots and bar plots to illustrate the enriched terms and pathways.

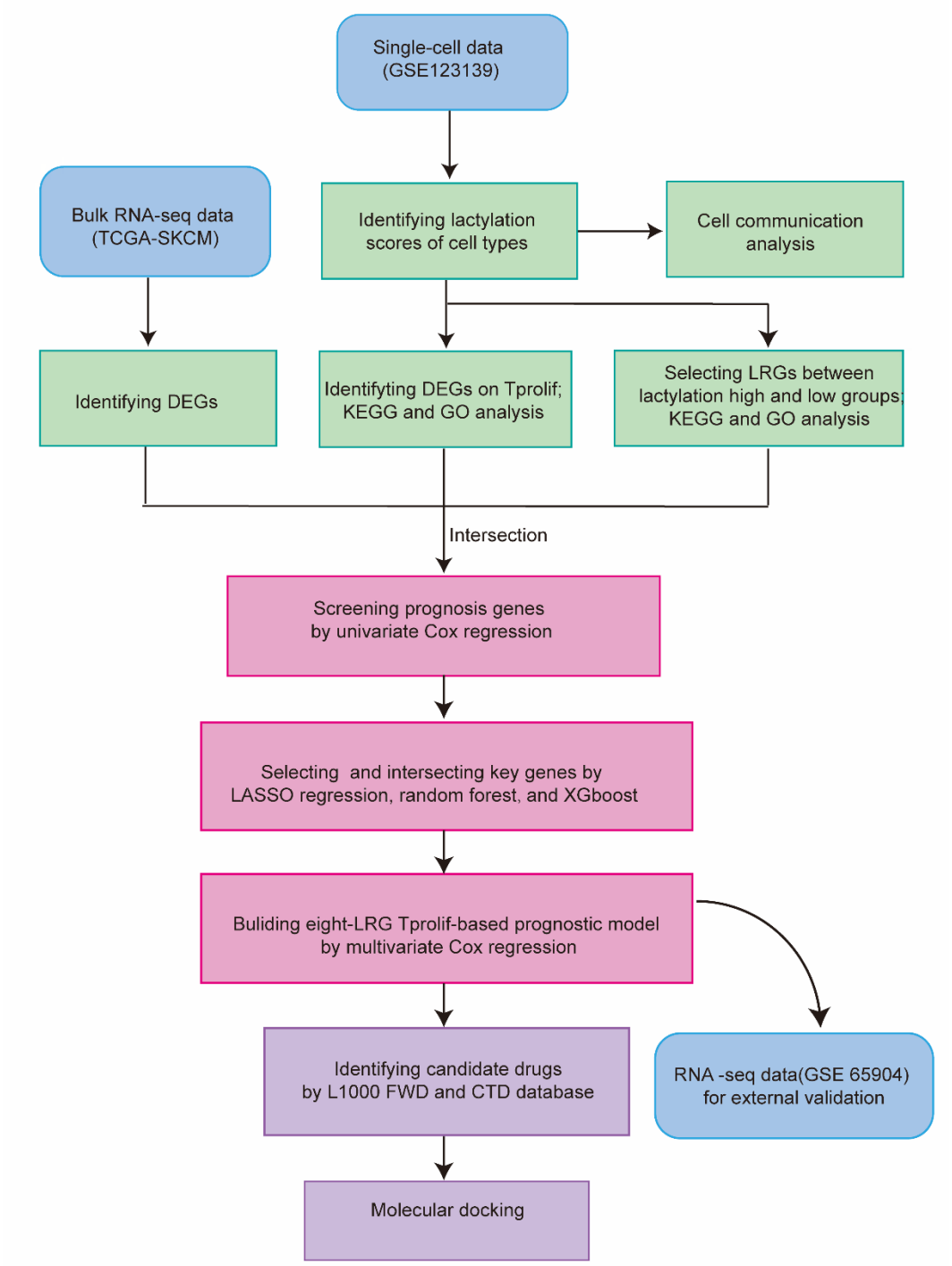


Figure 1. Workflow of data design
Abbreviations: CTD: Comparative Toxicogenomics Database; DEG: Differentially expressed gene; FWD: Fireworks Display; GO: Gene Ontology; KEGG: Kyoto Encyclopedia of Genes and Genomes; LASSO: Least absolute shrinkage and selection operator; LRG: Lactylation-related gene; RNA-seq: RNA sequencing; SKCM: Skin cutaneous melanoma; TCGA: The Cancer Genome Atlas.

2.6. Prognostic model construction based on multiple machine learning approaches

Univariate analysis was performed on a total of 66 intersection genes of DEGs of Tprolif, DEGs of TCGA-SKCM, and LRGs using the R package Survival[29], and 23 significant genes with $p < 0.05$ were selected. Subsequently, to improve the reliability of gene selection for the prognostic model, three machine learning methods, including the least absolute shrinkage and selection operator (LASSO)[30], random forests[31] and XGBoost[32] were performed on the 23 significant genes respectively. Finally, eight genes were selected for building a prognostic model via a multivariable Cox proportional hazards regression method. The risk score equation named lactylation of Tprolif-associated risk score of overall survival (LTRSO) was obtained based on the coefficients of the eight genes associated with prognosis in the regression model. According to the median value of LTRSO in TCGA-SKCM dataset (training set) and GSE65904 (validation set), the patients were divided into high-risk and low-risk group. Kaplan–Meier survival analysis was performed using the R package Survival. Time-dependent (one-, three-, and five-year) receiver operating characteristic (ROC) curves were also generated.

2.7. Identification of candidate drugs

The L1000 Fireworks Display (FWD) platform (https://maayanlab.cloud/l1000fwd/) is an essential resource in drug discovery research. In this study, eight key lactylation of Tprolif-associated genes that were upregulated or downregulated in SKCM were analyzed using the L1000 FWD tool. Through this analysis, we identified small molecules that demonstrated an inverse correlation with the expression profiles of these genes, thereby highlighting potential therapeutic agents for the treatment of SKCM.

The Comparative Toxicogenomic Database (CTD; http://ctdbase.org) was also utilized to identify additional candidate drugs for SKCM. In the CTD Batch Query Box, the eight genes in the prognostic model retrieved 2,563 chemicals (Table S6). Based on gene expression patterns, chemicals that displayed an inverse correlation with the eight DEGs and were not environmental pollutants were selected. Chemicals interacting with ≥3 key genes associated with SKCM were also selected through intersection analysis.

2.8. Molecular docking

Candidate drug molecules and their corresponding mol2 files were obtained from the PubChem database (https://pubchem.ncbi.nlm.nih. gov/), and the ligands were converted into the required PDBQT format using AutoDockTools.[33] Energy minimization was performed via Chem3D. The three-dimensional (3D) structures of the core targets were acquired from the Protein Data Bank (PDB) database (https://www.rcsb.org/) or the AlphaFoldDB database (https://alphafold.ebi.ac.uk/). PyMOL[34] was used for removing water molecules, heteroatoms, and ligands in the PDB files. After hydrogen atoms were added, the grid box of core targets was generated using AutoDockTools. Finally, the docking simulation was performed via AutoDock, and the results were visualized in PyMOL.

2.9. Statistical analysis

All statistical analyses were conducted using R software version 4.2.2. A p-value < 0.05 was considered statistically significant, unless specified otherwise. Survival analysis was performed using the R packages "survival" and "survminer".

3. Results

3.1. Tprolif exhibits the highest lactylation score in the tumor microenvironment

To identify the lactylation degree of various cell types in the TME of SKCM, the scRNA-seq dataset was obtained from the The Tumor Immune Single Cell Hub 2, and bioinformatic analysis was performed. There were 17 clusters under the resolution of 0.7 in the PCA map (Figure 2A), and the first 10 principal components were selected for UMAP analysis (Figure 2B). Afterwards, lactylation scores among cell types were assigned, and it was found that Tprolif is the cell type with the highest lactylation score, followed by cDC2 and fibroblast cells (Figure 2C and 2D).

Furthermore, to explore the enrichment pathways and biological processes of Tprolif, we performed KEGG and GO analysis for DEGs in Tprolif. The findings revealed that DEGs in Tprolif played vital roles in tumor-progression pathways such as cell adhesion molecules, cytoskeleton organization, and chromosome segregation, and were also associated with immune-related pathways such as Th1 and Th2 cell differentiation (Figure 2E and 2F).

3.2. Macrophage migration inhibitory factor signaling is the dominant intercellular communication pathway between Tprolif and other cell types

To further investigate the roles and connections across cell types in SKCM, intercellular communication analysis was performed. The findings demonstrate that exhausted $CD8^+$ T (CD8Tex) cells exhibited the greatest number of interactions and interaction weight with other cell types (Figure 3A and 3B). Furthermore, the top 20% of

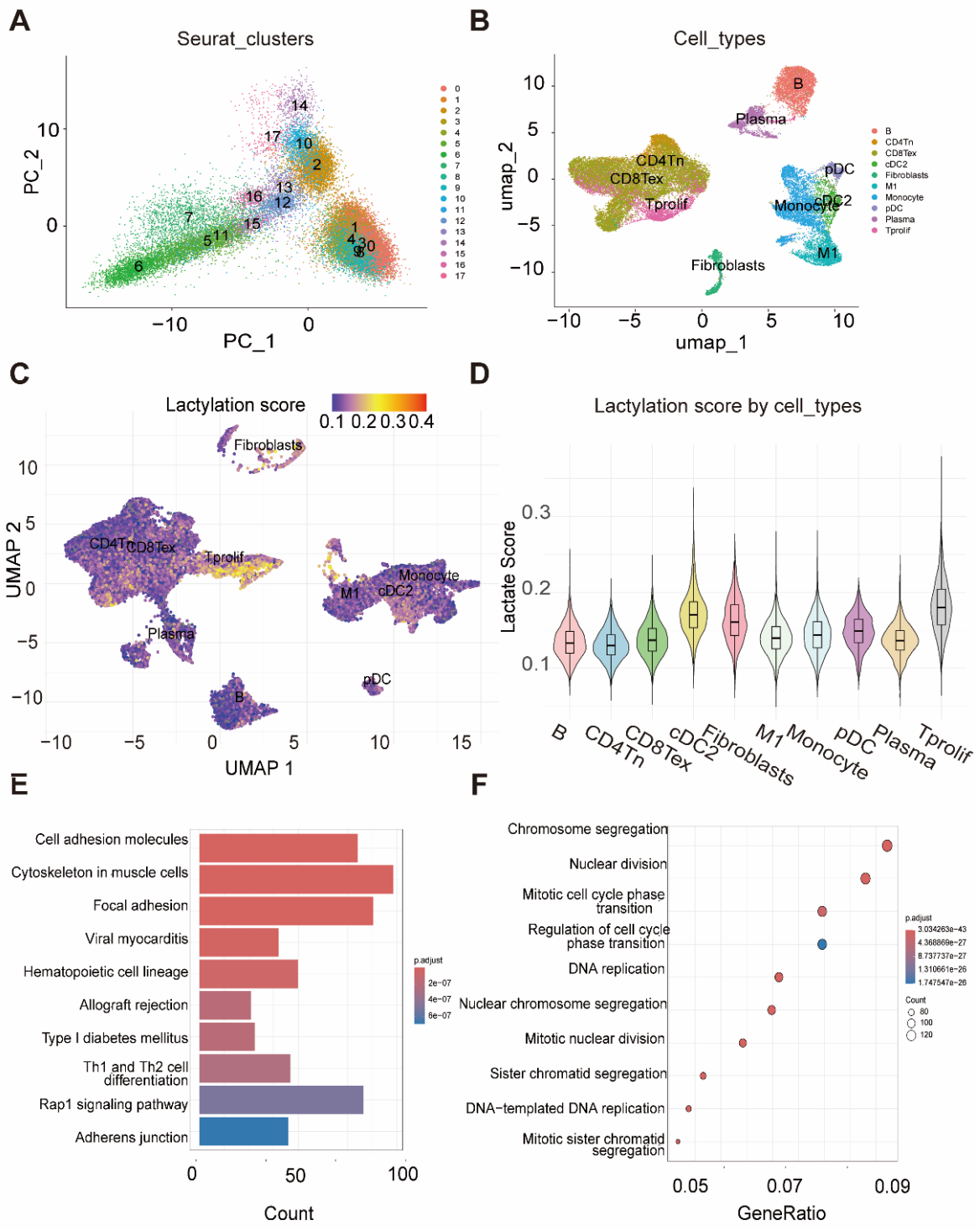


Figure 2. Identification of Tprolif as the cell type with the highest level of lactylation. (A) Principal component analysis of single-cell RNA sequencing data from SKCM samples, showing 18 clusters at a resolution of 0.7. (B) UMAP visualization of the same dataset, annotated into 10 major cell types based on known lineage markers. (C) UMAP plot colored by AUCell score for lactylation-related gene sets, where warmer colors indicate higher predicted lactylation activity. (D) Comparison of lactylation score across cell types. (E) Barplot visualization demonstrating Kyoto Encyclopedia of Genes and Genomes pathways in Tprolif cells. (F) Dot plot visualization demonstrating Gene Ontology biological process enrichment in Tprolif cells.
Abbreviations: CD8Tex: Exhausted CD8$^+$ T cell; pDC: Plasmacytoid dendritic cell; UMAP: Uniform manifold approximation and projection.

interactions ranked by interaction weight were analyzed, and the results indicated that CD8Tex interacted with almost all other immune cells except for plasmacytoid dendritic cells (Figure 3C).

As Tprolif was identified as the cell type with the highest lactylation score, we next explored the interactions between Tprolif and other cell types. The findings revealed that Tprolif had the most interactions with itself, followed by interactions with M1 macrophages and monocytes (Figure 3D). Using Tprolif as the signaling-sending cell type and other cell types as targets, the bubble plot indicated that Tprolif had the strongest interaction with CD8Tex through the MIF pathway (Figure 3E). MIF signaling pathway networks among cell types were plotted, which also showed a strong interaction between Tprolif and CD8Tex via the MIF signaling pathway (Figure 3F and 3G). A previous study identified MIF as an essential immune regulatory factor that can modulate immune cell function to suppress anti-tumor immune responses, thereby promoting tumor cell growth and metastasis.[35]

3.3. Identification of lactylation-related genes in Tprolif cells of skin cutaneous melanoma

To identify the genes that primarily reflect lactylation modification, we categorized all cells into two groups according to the median area under the curve score: high-lactylation and low-lactylation groups (Figure 4A). A total of 954 DEGs were identified after differential analysis. Moreover, Pearson's correlation analysis was performed to assess the relationship between the expression of each gene and lactylation scores, and the top 100 genes were then selected (Figure 4B). In total, 1,011 LRGs were identified by overlapping the DEGs with the top 100 genes. Subsequently, KEGG and GO enrichment analyses were performed to identify the pathways and biological functions predominantly associated with the LRGs (Figure 4C and 4D). The findings demonstrate that LRGs were mainly enriched in pathways related to cell cycle and chromosome segregation, indicating that LRGs may play a crucial role in tumor proliferation.

3.4. Construction of an eight-gene prognostic model based on lactylation-related genes in Tprolif cells

A total of 1,665 DEGs between tumor and normal tissues were identified in the TCGA-SKCM dataset (Table S5 and Figure S2). These DEGs were then intersected with the DEGs in Tprolif cells and LRGs, and a set of 66 common genes were obtained (Figure 4E and Table S7).

To select genes for building the prognostic model, we conducted univariate analysis of the 66 genes, resulting in the selection of 23 genes that exhibited significant associations with overall survival (Figure 5A). Following this, we employed multiple machine-learning approaches, including LASSO regression, random forest, and XGBoost, to further analyze these 23 genes. A total of 14 genes were selected via LASSO regression (Figure 5D), and the cross-validation plot and coefficient path plot were also visualized (Figure 5B and 5C).

After performing random forest and XGBoost analyses, the top 10 genes were selected based on their calculated feature importance (e.g., mean decrease Gini for random forest or gain for XGBoost), representing genes with the greatest contribution to model prediction (Figure 5E and 5F). Finally, we intersected the genes identified by the three machine learning methods, resulting in a set of eight genes: *MKI67*, *LMNA*, *RAI14*, *DOCK1*, *FABP5*, *ANKRD50*, *CBR3*, and *PAICS* (Figure 6A). These genes were used to construct a Cox multivariate risk prognostic model. The LTRS risk score was calculated as follows:

$$\begin{aligned} LTRSO = &\left(-0.01735 \times MKI67\right) \\ &+\left(0.0016 \times LMNA\right)-\left(0.01766 \times RAI14\right) \\ &-\left(0.03638 \times DOCK1\right)+\left(0.00489 \times FABP5\right) \\ &-\left(0.00682 \times ANKRD50\right)+\left(0.01426 \times CBR3\right) \\ &-\left(0.00771 \times PAICS\right) \end{aligned} \quad (1)$$

The forest plot revealed that *LMNA*, *DOCK1*, and *FABP5* were significantly associated with survival, indicating that these three genes are potential independent prognostic factors for SKCM (Figure 6B). Based on the median LTRSO, patients in the training set (TCGA-SKCM) were divided into high-risk and low-risk groups, and the findings show that patients in the low-risk group had a better prognosis that those in the high-risk group (Figure 6C).

To evaluate the diagnostic performance of this model, an ROC curve was plotted (Figure 6D), and the area under the ROC curve for one-, three, and five-year overall survival was 0.71, 0.712, and 0.68, respectively, demonstrating moderate prognostic performance, effectively distinguishing between different risk groups.

To assess the predictive value of our prognostic model, we conducted external validation with the GSE65904 dataset. The results indicated that our prognostic score robustly differentiated between high-risk and low-risk groups, further confirming its potential clinical utility (Figure 6E and 6F).

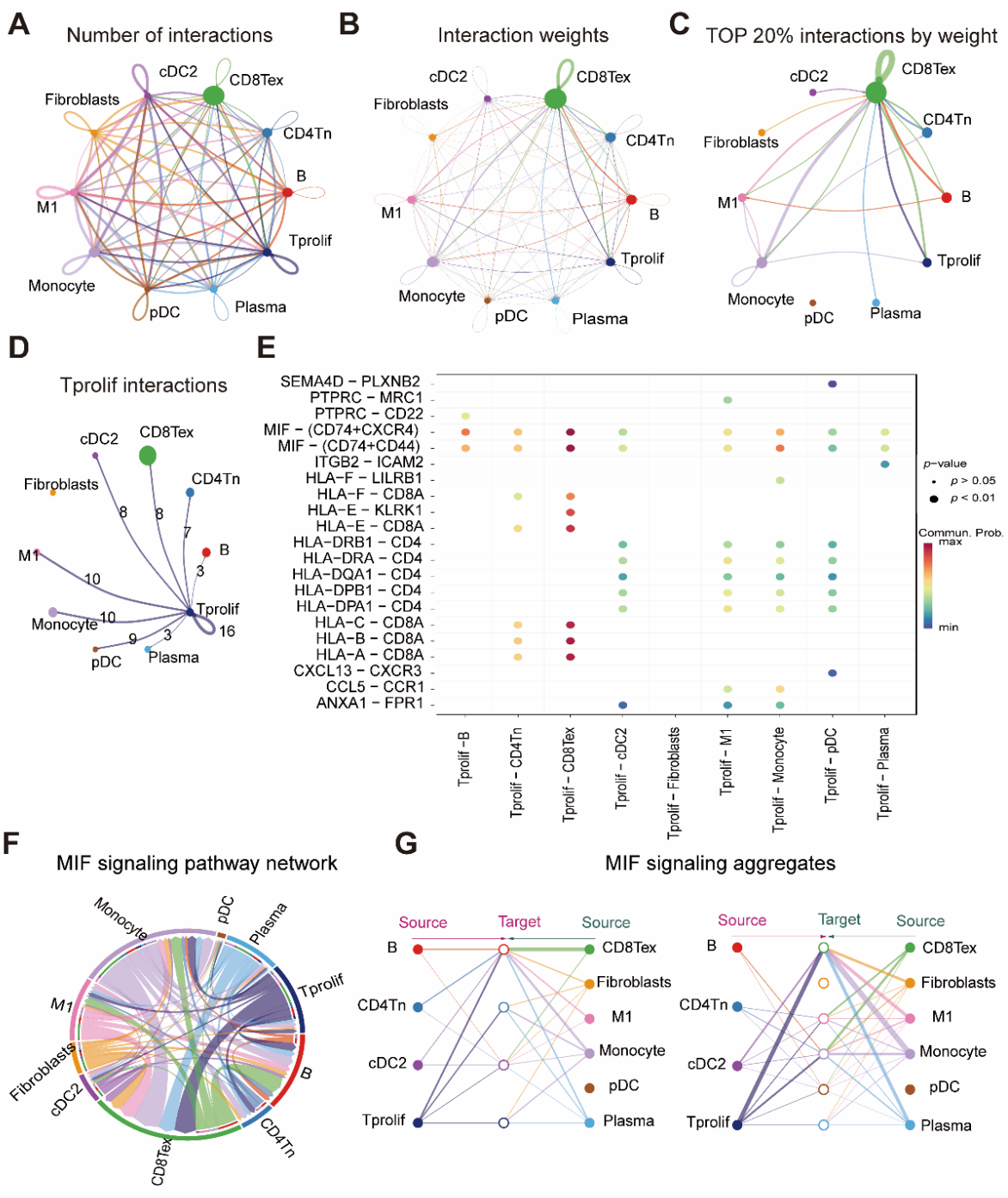


Figure 3. Cell–cell communication analysis. (A) Frequency of ligand–receptor interactions among different cell types. (B, C) Network diagrams illustrating (B) the total interaction weights and (C) top 20% of interaction weights among different cell types. (D) Ligand–receptor interactions between Tprolif and other cell types. (E) Bubble plot showing all ligand–receptor interactions between Tprolif and other cell types. (F) Chord diagram illustrating intercellular communication within the MIF signaling pathway. (G) Hierarchical network representation of MIF signaling pathway interactions across different cell types.

Abbreviations: CD8Tex: Exhausted CD8$^+$ T cell; MIF: Macrophage migration inhibitory factor; pDC: Plasmacytoid dendritic cell.

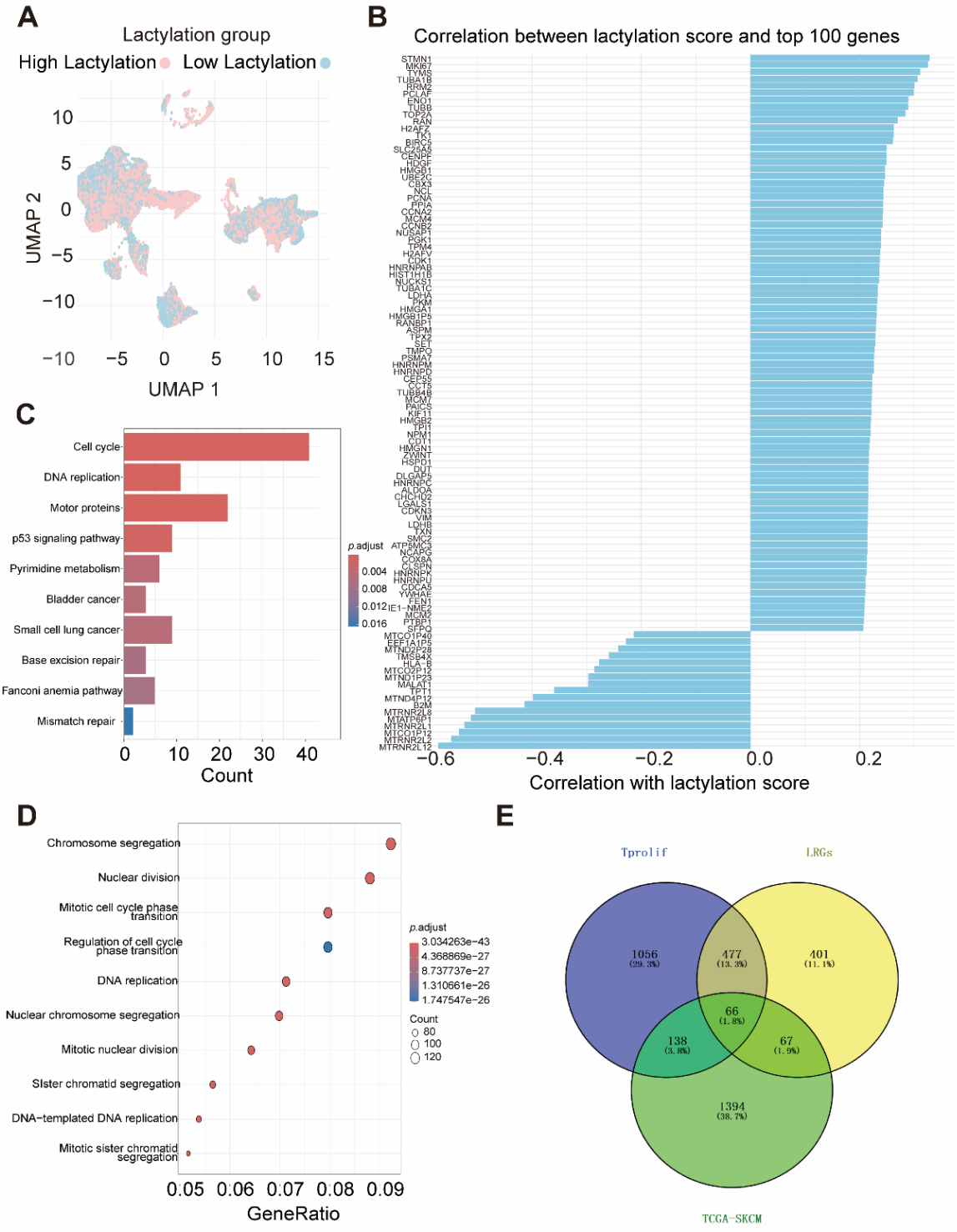


Figure 4. Identification of LRGs in SKCM. (A) UMAP visualization of the lactylation-associated cell group. (B) Top 100 genes associated with lactate score identified through correlation analysis between lactate score and gene expression. (C) Kyoto Encyclopedia of Genes and Genomes pathway enrichment analysis of LRGs. (D) Gene Ontology biological process enrichment analysis of LRGs. (E) Venn diagram illustrating the overlap among LRGs, significantly differentially expressed Tprolif genes, and significantly differentially expressed genes in the TCGA-SKCM dataset.

Abbreviations: LRG: Lactylation-related gene; SKCM: Skin cutaneous melanoma; TCGA: The Cancer Genome Atlas; UMAP: Uniform manifold approximation and projection.

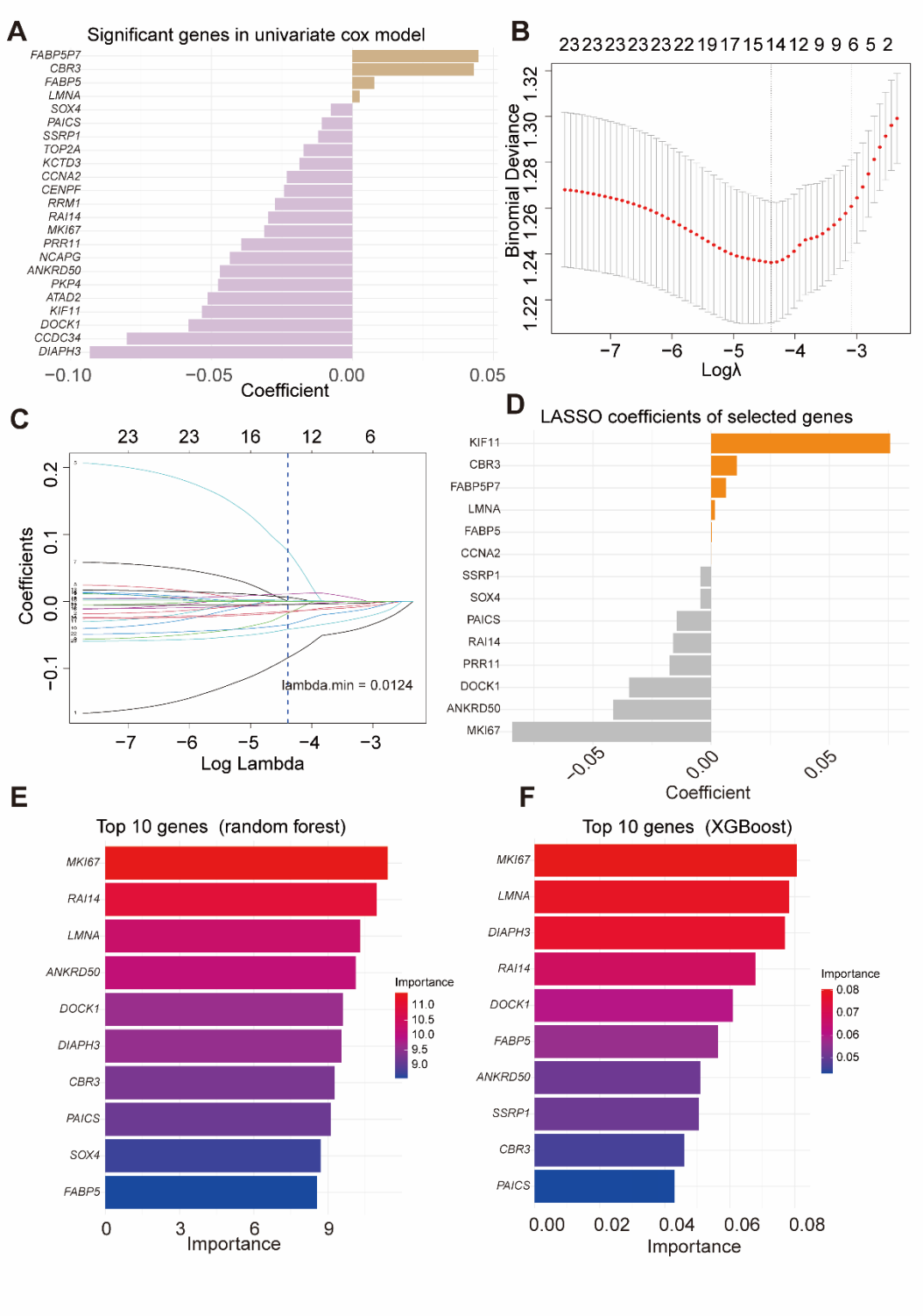


Figure 5. Selection of key genes for construction of the prognostic model. (A) Bar plot displaying genes identified as significant in the univariate Cox regression analysis. (B) Ten-fold cross-validation for optimal variable selection in LASSO regression analysis. (C) LASSO coefficient path illustrating gene selection across different penalty values. (D) Bar chart showing genes selected by LASSO regression. (E,F) Bar plots displaying the top 10 genes ranked by feature importance based on (E) XGBoost and (F) random forest.
Abbreviation: LASSO: Least absolute shrinkage and selection operator.

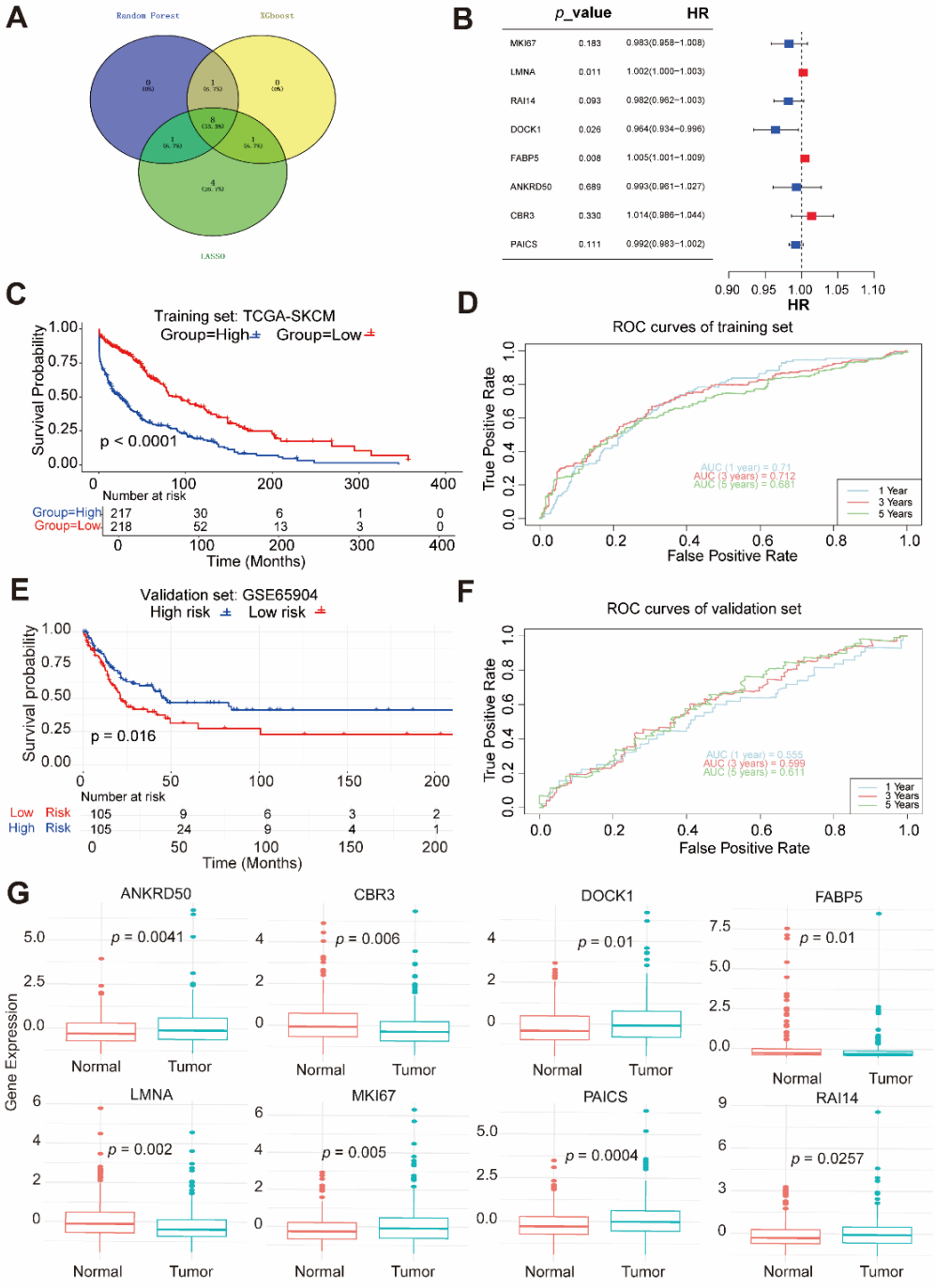


Figure 6. Training and validation of the eight-lactylation–related gene Tprolif-based prognostic model. (A) Venn diagram illustrating the overlap among the top 10 genes identified by random forest, top 10 genes identified by XGBoost, and genes selected by LASSO regression. (B) Forest plot showing results of multivariate Cox regression analysis. (C) Overall survival analysis in the TCGA-SKCM training dataset. (D) Time-dependent ROC curve assessing the prognostic performance of the model in the training cohort. (E) Overall survival analysis in the GSE65904 validation dataset. (F) Time-dependent ROC curve evaluating the prognostic performance of the model in the validation cohort. (G) Comparison of mRNA expression levels of the eight prognostic genes between normal and tumor tissues.

Abbreviations: HR: Hazard ratio; LASSO: Least absolute shrinkage and selection operator; ROC: Receiver operating characteristic; SKCM: Skin cutaneous melanoma; TCGA: The Cancer Genome Atlas.

3.5. Screening of drug candidates

Since the selection of candidate drug molecules was based on gene expression patterns, we first examined the expression profiles of the eight genes in both tumor and normal tissues. The findings demonstrate that five genes were upregulated and three genes were downregulated in tumor tissues (Figure 6G). Next, the L1000 FWD online application was utilized to search for the five upregulated genes and three downregulated genes. Candidate drug molecules were selected based on their opposite correlations with the identified genes, considering factors such as similarity score, *p*-value, and combined score, as detailed in Table 1. BG-FA-0953 showed the highest combined score, suggesting that it might be the most promising candidate for treating SKCM.

To identify additional candidate drugs targeting the eight LRGs in Tprolif cells for combination therapy in SKCM, we constructed gene–chemical and gene–chemical–disease networks based on the CTD database (Figure 7A–7I). The results indicate that 58 candidate drugs were associated with the key genes (Table S8), and candidate drugs with more than three common target genes are listed (Table 2 and Figure 7I). Valproic acid (VPA), cyclosporine, *Jinfukang*, and ivermectin were identified as potential candidate agents for further investigation in SKCM, based on their predicted interactions with the eight LRGs. These computational predictions require experimental validation in future studies. *Jinfukang* is a traditional Chinese medicine compound, which is typically composed of multiple herbal ingredients.

3.6. Molecule docking between BG-FA-0953 and the eight lactylation-related genes in Tprolif cells

Detailed information regarding BG-FA-0953 (Pubchem CID: 6446335) was retrieved from the PubChem database. Its properties include a molecular weight of 294.26 g/mol, a molecular formula of $C_{15}H_{10}N_4O_3$, and its two-dimensional structure is illustrated in Figure S3. The SDF file of BG-FA-0953 was downloaded from the PubChem database to be used as a ligand in molecular docking analysis.

The 3D structures of the target receptors include MKI67 (PDB: 5j28), LMNA (AlphaFoldDB: AF-P02545-F1-v4), RAI14 (AlphaFoldDB: AF-Q9P0K7-F1-v4), DOCK1 (PDB: 3l4c), FABP5 (PDB: 1b56), ANKRD50 (AlphaFoldDB: AF-Q9ULJ7-F1-v4), CBR3 (PDB: 2hrb), and PAICS (PDB:2h31). A docking score lower than −7 kcal/mol is regarded as indicative of a strong binding affinity, while scores below −4.25 kcal/mol suggest good affinity. Additionally, a score below 0 kcal/mol is often interpreted as a sign of potential spontaneous binding between the ligand and the target protein.[36]

Our docking results revealed that BG-FA-0953 exhibited good binding affinity with all target receptors and strong binding affinity with ANKRD50, CBR3, DOCK1, MKI67, and PAICS (Figure 8A). Moreover, we found that BG-FA-0953 and target proteins are mainly stabilized through hydrogen bonding interactions. The compound formed a hydrogen bond with GLU-307 in ANKRD50 at 3.5 Å. In CBR3, three hydrogen bonds were formed: one with ILE-17 at 3.3 Å and two with ASN-90 at 3.2 and 3.5 Å. For DOCK1, four hydrogen bonds were observed: one with GLN-488 at 3.3 Å and three with LYS-487 at 2.9, 3.1, and 3.1 Å. For FABP5, two hydrogen bonds were observed: one with ALA-39 at 3.5 Å and another with ALA-37 at 3.3 Å. In LMNA, five hydrogen bonds were observed: one with THR-480 at 3.4 Å and four with TRP14 or SER516 at distances of 2.8, 3.3, 3.2, and 2.8 Å. MKI67 formed three hydrogen bonds with GLU-218, ASP-220, and ASP-208 at 3.5, 3.1, and 3.1 Å, respectively. In PAICS, six hydrogen bonds were formed with ASP-212, ASP-211, ARG-215, and ARG-101. Finally, RAI14 exhibited two hydrogen bonds with ASP-83 and THR-85 at 2.1 and 3.5 Å, respectively (Figure 8B–8I).

4. Discussion

In this study, we first identified Tprolif as the cell type with the highest lactylation score in the TME of SKCM, highlighting its potential involvement in shaping the immunosuppressive TME. Additionally, the MIF ligand–receptor pathway was identified as the most significant communication pathway between Tprolif and other cell types, suggesting a potential connection between the MIF pathway and lactylation-related processes in the TME. After intersecting DEGs in Tprolif, DEGs in TCGA-SKCM, and LRGs, an eight-LRG Tprolif-based prognostic model was constructed for risk stratification in SKCM patients. Various algorithms, including LASSO regression, random forest, and XGBoost were employed for model building, aiming to enhance the model's accuracy, stability, and generalizability. Furthermore, several therapeutic candidates were identified for SKCM based on the expression pattern of eight LRGs, including BG-FA-0953, VPA, cyclosporine, ivermectin, and *Jinfukang*. Unlike the other four candidates, *Jinfukang* is a type of traditional Chinese medicine comprised of 10 ingredients. We finally performed molecular docking to evaluate the binding affinities between BG-FA-0953 and its targets.

Tprolif is a dynamic and proliferative subset of T cells. T cell proliferation is a key part of the immune response, where T cells transition from a quiescent to an active proliferative state in response to specific stimuli. This process occurs when T cells interact with antigen-presenting cells, activating signaling pathways that induce proliferation.[37] It also plays a crucial role in the TME by

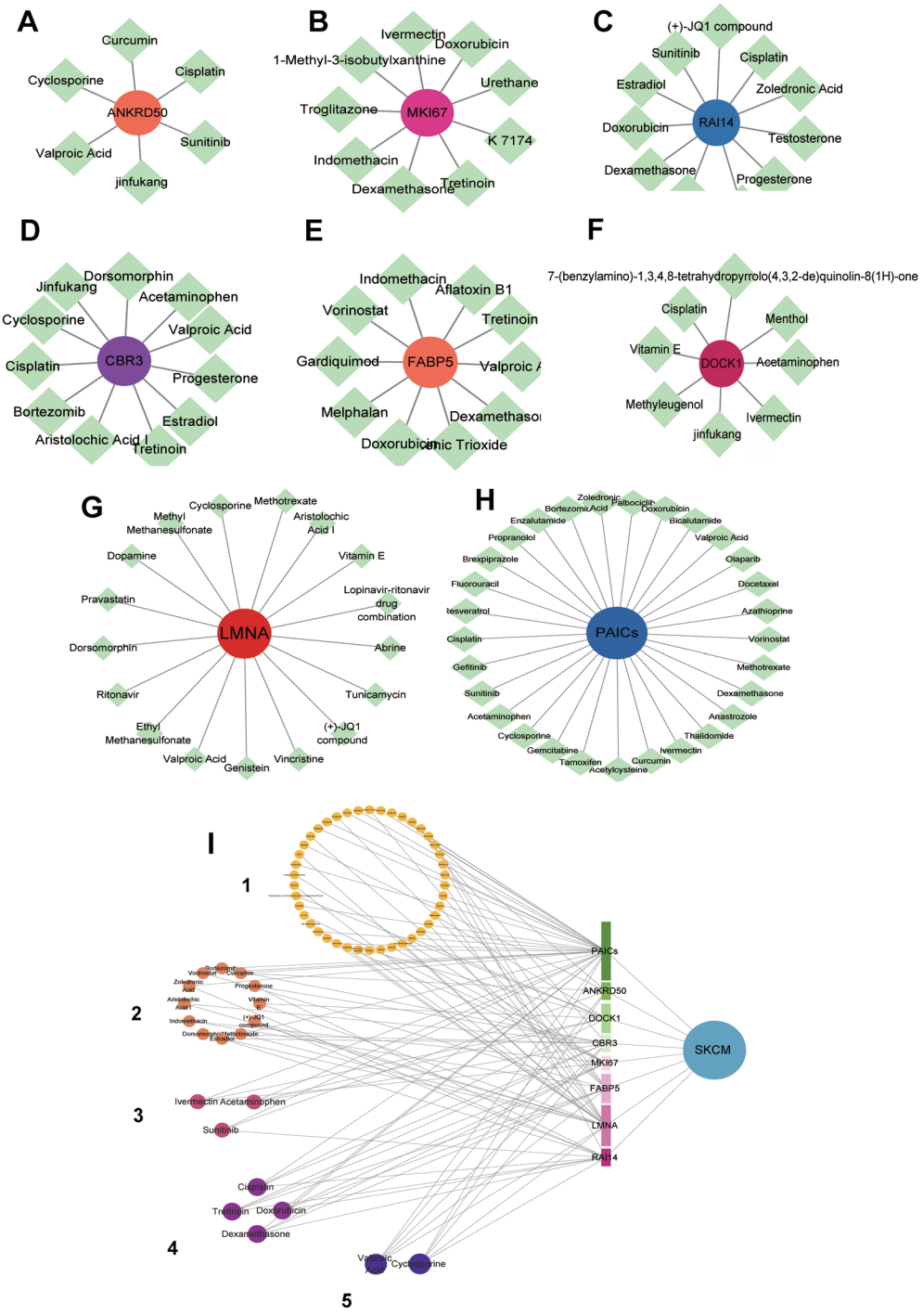


Figure 7. Chemical–gene–SKCM interaction network. (A–H) Chemical–gene interaction analyses across different compounds. (I) Predicted chemical–gene–SKCM interaction network.
Abbreviation: SKCM: Skin cutaneous melanoma.

Table 1. Drugs with inverse correlation identified from the L1000 FWD database

Rank	Drug	Similarity score	*p*-value	*q*-value	*Z*-score	Combined score
1	BG-FA-0953	−0.5714	0.0000022*	0.0177	1.79	−10.11
2	Amsacrine	−0.5714	0.00000351*	0.0177	1.82	−9.94
3	Mitomycin-c	−0.5714	0.00000462*	0.0198	1.8	−9.6
4	Fludarabine	−0.5714	0.00000294*	0.0177	1.68	−9.32
5	Celastrol	−0.5714	0.00000294*	0.0177	1.66	−9.2
6	BRD-K77547920	−0.4286	0.000126*	0.0555	1.84	−7.16
7	Lenalidomide	−0.4286	0.00014*	0.0555	1.85	−7.13
8	BRD-K73125384	−0.4286	0.000137*	0.0555	1.84	−7.11
9	Auranofin	−0.4286	0.00015*	0.0555	1.83	−7.01
10	Simvastatin	−0.4286	0.000153*	0.0555	1.84	−7.01

Note: *$p < 0.05$ indicates statistical significance.

Table 2. Candidate drugs with interactions involving ≥3 key genes

Candidate drug	Interacted key gene count	Interacted key gene	Clinical application
Cisplatin	5	*ANKRD50*, *DOCK1*, *PAICS*, *RAI14*, *CBR3*	Anti-cancer
Valproic acid	5	*ANKRD50*, *PAICS*, *FABP5*, *CBR3*, *LMNA*	Anticonvulsant
Cyclosporine	5	*ANKRD50*, *PAICS*, *RAI14*, *LMNA*, *CBR3*	Immunosuppressive
Dexamethasone	4	*PAICS*, *MKI67*, *RAI14*, *FABP5*	Adjunctive anti-cancer
Doxorubicin	4	*PAICS*, *MKI67*, *RAI14*, *FABP5*	Anti-cancer
Tretinoin	4	*PAICS*, *MKI67*, *RAI14*, *CBR3*	Anti-cancer
Jinfukang	3	*ANKRD50*, *DOCK1*, *CBR3*	Traditional Chinese medicine
Sunitinib	3	*ANKRD50*, *PAICS*, *RAI14*	Anti-cancer
Ivermectin	3	*DOCK1*, *PAICS*, *MKI67*	Anti-parasitic

enabling the immune system to recognize and eliminate tumor cells, whereas tumor cells often induce immune suppression in the TME, limiting T cell proliferation and facilitating immune evasion.[38,39]

As one of the most significant metabolites, lactate is typically present at high concentrations of up to 40 mM in the TME[40], while its concentration is only in the range of 1.5 to 3 mM in blood and healthy tissues.[41] Lactate concentration in various tumor regions is strongly correlated with tumor metastasis, with elevated lactate levels being indicative of a greater propensity for metastasis.[42] In 2019, Zhang *et al.*[17] discovered a novel histone modification called lactylation, which was induced by lactate on histone lysine residues. This modification acts as an epigenetic change in chromatin, directly stimulating gene transcription. Recently, several studies have reported that lactylation plays a pivotal role in regulating T cell proliferation and function in the TME, especially within the context of immune activation. For example, Fischer *et al.*[43] demonstrated that high lactate concentration in the TME inhibits T cell proliferation and function. Additionally, Raychaudhuri *et al.*[44] demonstrated that H3K18 lactylation (H3K18la) and H3K9 lactylation (H3K9la) are enriched in $CD8^+$ T cells, and modulation of H3K18la as well as H3K9la influences $CD8^+$ T cell effector function in the TME.

In this study, we found that Tprolif cells exhibited higher lactylation scores compared to other cell types. This observation leads us to hypothesize that lactylation may contribute to tumor immune suppression by modulating the proliferation or function of Tprolif cells in the SKCM TME. However, direct evidence of such a mechanism is currently lacking. Based on the marker analysis, Tprolif cells in SKCM exhibited a proliferative exhausted phenotype ($MKI67^+PDCD1^+TOX^+$), distinct from naïve or central memory T cells. This suggests that lactylation may regulate the exhausted proliferative state in the TME.

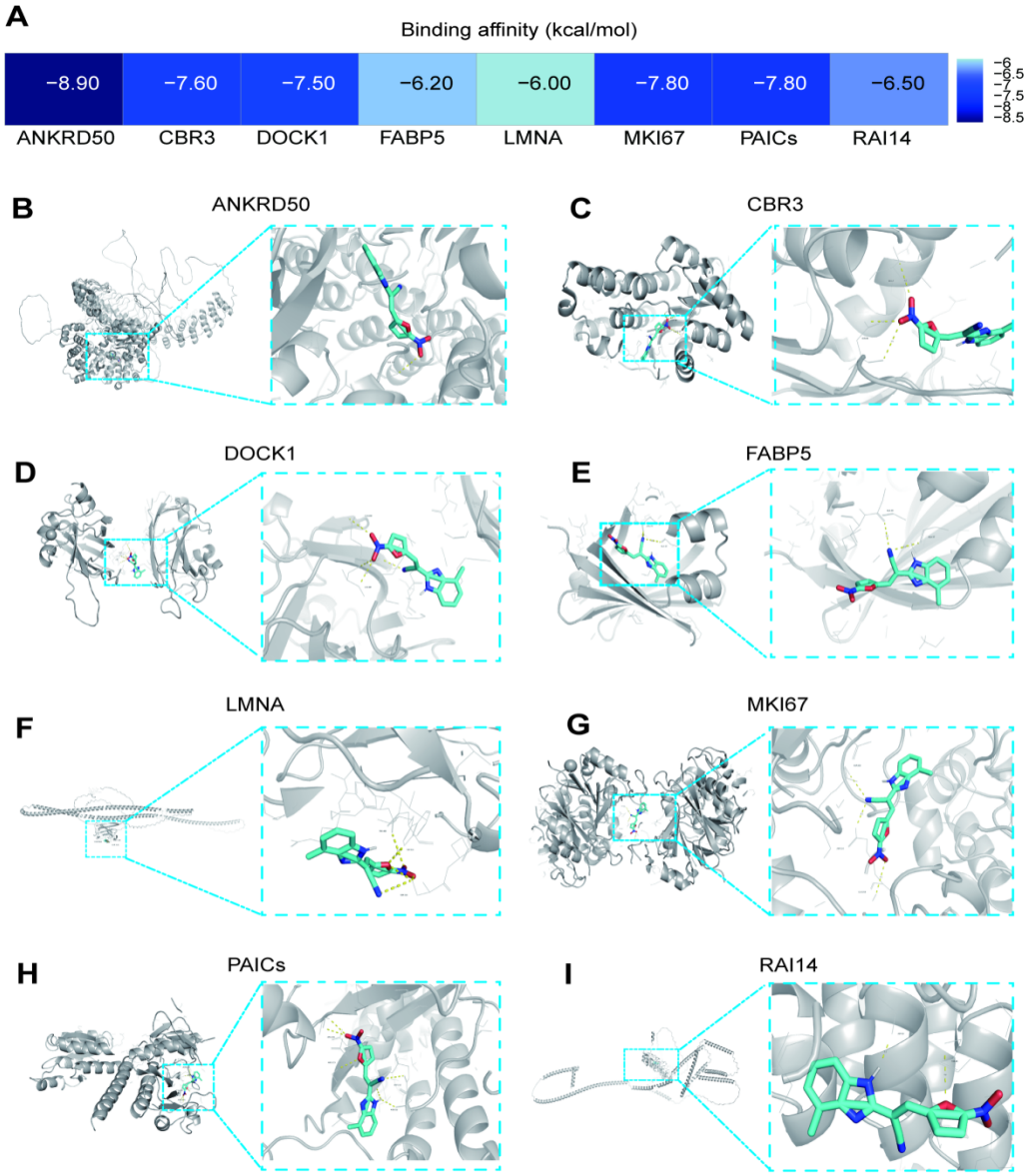


Figure 8. Molecular docking analysis of BG-FA-0953 with target proteins. Hydrogen bonds are indicated by yellow dashed lines. BG-FA-0953 is shown in blue, and target proteins are shown in gray. The number and length of hydrogen bonds may be used to evaluate the strength of molecular interactions.

As a type of cytokine involved in protein interaction, MIF plays a central role in immune and inflammatory responses.[35] Previous studies have demonstrated that MIF is correlated with worse prognosis of multiple cancers—including lung cancers, gastric cancers, and breast cancers[45-47]—and is associated with immune suppression in the TME. Recently, Zhu *et al.*[48] found that MIF exhibits high expression in $CD36^+$ cancer-associated fibroblasts, and MIF can recruit $CD33^+$ myeloid-derived suppressor cells to promote an immunosuppressive TME in hepatocellular carcinoma. In another study, Jia *et al.*[49] developed an MIF tautomerase inhibitor, which could effectively inhibit differentiation of myeloid-derived suppressor cells and thereby reverse the immunosuppressive microenvironment of pancreatic cancer. Moreover, Cohen Shvefel *et al.*[50] analyzed the mechanisms of immune escape with low intra-tumor heterogeneity. They identified MIF as a key factor of immune rejection in tumors with intra-tumor

heterogeneity, which was validated in data from melanoma patients.

In the present study, we found that the MIF-mediated interaction between Tprolif and CD8Tex cells was the most significant pathway. Based on these communication data, we speculate that highly lactylated Tprolif cells may express MIF to recruit CD8Tex cells, thereby potentially promoting an immunosuppressive microenvironment. This hypothesis remains to be tested experimentally. At present, due to the limitations of experimental conditions and time, we cannot conduct wet experiments in this research. In the future, we hope to verify this hypothesis through experimental validation.

Our ultimate goal is to identify potential therapeutic candidates and support the development of clinical treatments for SKCM. In this study, we identified the top 10 potential therapeutic small molecules for SKCM, led by BG-FA-0953 based on the L1000 FWD platform. Additionally, we explored other drug candidates for SKCM, including VPA, cyclosporine, ivermectin, and *Jinfukang* based on the CTD database. VPA is a type of histone deacetylase inhibitor, which was originally developed as an antiepileptic drug in the clinic and demonstrated antitumor functions in various cancers, including pancreatic cancer and breast cancer.[51,52] Although previous report has demonstrated that VPA can induce apoptosis in melanoma cells and VPA exposure might be associated with reduced melanoma risk and progression[53], no study has yet explicitly illustrated VPA's potential as a combination therapeutic agent for SKCM through anti-lactylation mechanisms.

Cyclosporine is a well-known immunosuppressant that can be used for transplantation anti-rejection, immune diseases, and refractory nephrotic syndrome. In recent years, cyclosporine was demonstrated to have great potential to reverse tumor resistance[54], while the therapeutic effect and mechanism of cyclosporine in SKCM are not clearly elucidated. As a broad-spectrum antiparasitic drug, ivermectin is also a potential anti-cancer agent. For example, Liu *et al.*[55] reported that ivermectin can inhibit the growth of esophageal squamous cell carcinoma through the activation of the activating transcription factor 4-mediated endoplasmic reticulum stress–autophagy pathway. Nevertheless, no studies have illustrated the therapeutic functions of ivermectin in SKCM.

Unlike other candidates, *Jinfukang* is a traditional Chinese medicine and a potential drug for lung cancer therapy.[56] Here, we suggest *Jinfukang* might be a candidate drug for SKCM through potentially regulating lactylation pathways in the TME of SKCM.

We performed molecular docking to demonstrate good binding affinities between BG-FA-0953 and its targets, although pharmacodynamic and toxicological experiments should be performed to verify its feasibility. The findings of the present study reveal that there is no commercial BG-FA-0953 at present.

It is important to acknowledge two main limitations of this study. First, lactylation scores were derived from transcriptomic signatures of LRGs rather than from direct protein lactylation assays. Therefore, our conclusions regarding the lactylation status of Tprolif cells should be interpreted as correlative and hypothesis-generating, pending experimental validation. Second, all drug predictions—including the identification of BG-FA-0953 and other candidate agents such as VPA, cyclosporine, ivermectin, and *Jinfukang*—are based solely on bioinformatic analyses and molecular docking, without any functional or pharmacological validation. Consequently, these predictions should be viewed as hypothesis-generating rather than clinically actionable. Collectively, while our computational findings provide valuable insights into lactylation-driven immune modulation and potential therapeutic avenues in SKCM, experimental confirmation is essential to substantiate these observations.

5. Conclusion

The findings suggest that Tprolif is the cell type with the highest lactylation score in the TME of SKCM, potentially indicating its role in shaping an immunosuppressive TME. After cell communication analysis, the MIF ligand–receptor pathway was identified as the key communication route between Tprolif and other cell types, linking lactylation-related processes to immune modulation. Furthermore, we developed an eight-LRG prognostic model via three machine learning methods. Based on the eight gene expression patterns, potential therapeutic candidates, including BG-FA-0953, VPA, cyclosporine, ivermectin, and *Jinfukang*, were identified. Molecular docking further confirmed good binding affinities of BG-FA-0953 with its targets. In summary, our study offers preliminary insights into immune modulation driven by lactylation, suggesting new opportunities that require experimental validation for prognostic assessment and therapeutic strategies in SKCM.

Acknowledgments

None.

Funding

This work was supported by the Research Development Fund for Talent Startup Project of Jiyang College, Zhejiang A&F University (grant number: RC2025F02), and the

General Scientific Research Project of Zhejiang Provincial Department of Education in 2025 (Y202558493).

Conflict of interest

The authors declare that they have no conflict of interest related to this study.

Author contributions

Conceptualization: Qianyu Shen, Sirui Qian, Yanan Yan, Maorong Suo, Yuan Wu
Data curations: Qianyu Shen, Sirui Qian, Yanan Yan, Xinhan Wu, Yingjia Ni, Maorong Suo
Formal analysis: Qianyu Shen, Sirui Qian, Yanan Yan, Xinhan Wu, Yingjia Ni, Maorong Suo
Supervision: Yuan Wu
Writing–original draft: Qianyu Shen, Sirui Qian
Writing–review & editing: Yuan Wu

Ethics approval and consent to participate

Not applicable.

Consent for publication

Not applicable.

Availability of data

The public RNA-sequencing datasets used in this study are available from the Gene Expression Omnibus and The Cancer Genome Atlas databases under the accession numbers GSE123139, GSE65904, and the TCGA-SKCM cohort, respectively.

References

1. Long GV, Swetter SM, Menzies AM, *et al*. Cutaneous melanoma. *Lancet*. 2023;402(10400):485-502.

   doi: 10.1016/S0140-6736(23)00821-8

2. Leonardi G, Falzone L, Salemi R, *et al*. Cutaneous melanoma: From pathogenesis to therapy (Review). *Int J Oncol*. 2018;52(4):1071-1080.

   doi: 10.3892/ijo.2018.4287

3. Gordon D, Hansson J, Eloranta S, *et al*. Primary tumor sites in relation to ultraviolet radiation exposure and skin visibility correlate with survival in cutaneous melanoma. *Int J Cancer*. 2017;141(7):1345-1354.

   doi: 10.1002/ijc.30843

4. Davis LE, Shalin SC, Tackett AJ. Current state of melanoma diagnosis and treatment. *Cancer Biol Ther*. 2019;20(11):1366-1379.

   doi: 10.1080/15384047.2019.1640032

5. Eriksson H, Utjés D, Olofsson Bagge R, *et al*. The Proportion Cured of Patients with Resected Stage II-III Cutaneous Melanoma in Sweden. *Cancers*. 2021;13(10):2456.

   doi: 10.3390/cancers13102456

6. Țăpoi DA, Derewicz D, Gheorghișan-Gălățeanu AA, *et al*. The Impact of Clinical and Histopathological Factors on Disease Progression and Survival in Thick Cutaneous Melanomas. *Biomedicines*. 2023;11(10):2616.

   doi: 10.3390/biomedicines11102616

7. Larkin J, Chiarion-Sileni V, Gonzalez R, *et al*. Five-Year Survival with Combined Nivolumab and Ipilimumab in Advanced Melanoma. *N Engl J Med*. 2019;381(16):1535-1546.

   doi: 10.1056/NEJMoa1910836

8. Klobuch S, Seijkens TTP, Schumacher TN, *et al*. Tumour-infiltrating lymphocyte therapy for patients with advanced-stage melanoma. *Nat Rev Clin Oncol*. 2024;21(3):173-184.

   doi: 10.1038/s41571-023-00848-w

9. Gide TN, Wilmott JS, Scolyer RA, *et al*. Primary and Acquired Resistance to Immune Checkpoint Inhibitors in Metastatic Melanoma. *Clin Cancer Res*. 2018;24(6):1260-1270.

   doi: 10.1158/1078-0432.CCR-17-2267

10. Jenkins RW, Barbie DA, Flaherty KT. Mechanisms of resistance to immune checkpoint inhibitors. *Br J Cancer*. 2018;118(1):9-16.

    doi: 10.1038/bjc.2017.434

11. Pitt JM, Vétizou M, Daillère R, *et al*. Resistance Mechanisms to Immune-Checkpoint Blockade in Cancer: Tumor-Intrinsic and -Extrinsic Factors. *Immunity*. 2016;44(6):1255-1269.

    doi: 10.1016/j.immuni.2016.06.001

12. Durante MA, Rodriguez DA, Kurtenbach S, *et al*. Single-cell analysis reveals new evolutionary complexity in uveal melanoma. *Nat Commun*. 2020;11(1).

    doi: 10.1038/s41467-019-14256-1

13. Quek C, Pratapa A, Bai X, *et al*. Single-cell spatial multiomics reveals tumor microenvironment vulnerabilities in cancer resistance to immunotherapy. *Cell Rep*. 2024;43(7):114392.

    doi: 10.1016/j.celrep.2024.114392

14. Marzagalli M, Ebelt ND, Manuel ER. Unraveling the crosstalk between melanoma and immune cells in the tumor microenvironment. *Semin Cancer Biol*. 2019;59:236-250.

    doi: 10.1016/j.semcancer.2019.08.002

15. Yang Z, Zheng Y, Gao Q. Lysine lactylation in the regulation of tumor biology. *Trends Endocrinol Metab*. 2024;35(8):720-731.

    doi: 10.1016/j.tem.2024.01.011

16. Li H, Sun L, Gao P, *et al*. Lactylation in cancer: Current understanding and challenges. *Cancer Cell*. 2024;42(11):1803-1807.

doi: 10.1016/j.ccell.2024.09.006

17. Zhang D, Tang Z, Huang H, *et al*. Metabolic regulation of gene expression by histone lactylation. *Nature*. 2019;574(7779):575-580.

doi: 10.1038/s41586-019-1678-1

18. Gu J, Xu X, Li X, *et al*. Tumor-resident microbiota contributes to colorectal cancer liver metastasis by lactylation and immune modulation. *Oncogene*. 2024;43(31):2389-2404.

doi: 10.1038/s41388-024-03080-7

19. Xiong J, He J, Zhu J, *et al*. Lactylation-driven METTL3-mediated RNA m(6)A modification promotes immunosuppression of tumor-infiltrating myeloid cells. *Mol Cell*. 2022;82(9):1660-1677.e10.

doi: 10.1016/j.molcel.2022.02.033

20. Li G, Wang D, Zhai Y, *et al*. Glycometabolic reprogramming-induced XRCC1 lactylation confers therapeutic resistance in ALDH1A3-overexpressing glioblastoma. *Cell Metab*. 2024;36(8):1696-1710.e10.

doi: 10.1016/j.cmet.2024.07.011

21. Han Y, Wang Y, Dong X, *et al*. TISCH2: expanded datasets and new tools for single-cell transcriptome analyses of the tumor microenvironment. *Nucleic Acids Res*. 2023;51(D1):D1425-D1431.

doi: 10.1093/nar/gkac959

22. Subramanian A, Tamayo P, Mootha VK, *et al*. Gene set enrichment analysis: a knowledge-based approach for interpreting genome-wide expression profiles. *Proc Natl Acad Sci USA*. 2005;102(43):15545-15550.

doi: 10.1073/pnas.0506580102

23. Hao Y, Hao S, Andersen-Nissen E, *et al*. Integrated analysis of multimodal single-cell data. *Cell*. 2021;184(13):3573-3587.e29.

doi: 10.1016/j.cell.2021.04.048

24. Wickham H. Navarro D, Pedersen TL, *ggplot2: Elegant Graphics for Data Analysis*. 2016. https://ggplot2-book.org/

25. Jin S, Guerrero-Juarez CF, Zhang L, *et al*. Inference and analysis of cell-cell communication using CellChat. *Nat Commun*. 2021;12(1).

doi: 10.1038/s41467-021-21246-9

26. Colaprico A, Silva TC, Olsen C, *et al*. TCGAbiolinks: an R/Bioconductor package for integrative analysis of TCGA data. *Nucleic Acids Res*. 2016;44(8):e71.

doi: 10.1093/nar/gkv1507

27. Ritchie ME, Phipson B, Wu D, *et al*. limma powers differential expression analyses for RNA-sequencing and microarray studies. *Nucleic Acids Res*. 2015;43(7):e47.

doi: 10.1093/nar/gkv007

28. Yu G, Wang LG, Han Y, *et al*. clusterProfiler: an R package for comparing biological themes among gene clusters. *OMICS: A Journal of Integrative Biology*. 2012;16(5):284-287.

doi: 10.1089/omi.2011.0118

29. Xie Y, Zhang J, Li M, *et al*. Identification of Lactate-Related Gene Signature for Prediction of Progression and Immunotherapeutic Response in Skin Cutaneous Melanoma. *Front. Oncol*. 2022;12.

doi: 10.3389/fonc.2022.818868

30. Friedman J, Hastie T, Tibshirani R. Regularization Paths for Generalized Linear Models via Coordinate Descent. *J Stat Soft*. 2010;33(1).

doi: 10.18637/jss.v033.i01

31. Strobl C, Boulesteix AL, Zeileis A, *et al*. Bias in random forest variable importance measures: illustrations, sources and a solution. *BMC Bioinformatics*. 2007;8(1).

doi: 10.1186/1471-2105-8-25

32. Chen T, Guestrin C. XGBoost. In: *Proceedings of the 22nd ACM SIGKDD International Conference on Knowledge Discovery and Data Mining*. ACM; 2016:785-794.

doi: 10.1145/2939672.2939785

33. Morris GM, Huey R, Lindstrom W, *et al*. AutoDock4 and AutoDockTools4: Automated docking with selective receptor flexibility. *J Comput Chem*. 2009;30(16):2785-2791.

doi: 10.1002/jcc.21256

34. Rauf MA, Zubair S, Azhar A. Ligand docking and binding site analysis with pymol and autodock/vina. *IJBAS*. 2015;4(2):168-177.

doi: 10.14419/ijbas.v4i2.4123

35. Sumaiya K, Langford D, Natarajaseenivasan K, Shanmughapriya S. Macrophage migration inhibitory factor (MIF): A multifaceted cytokine regulated by genetic and physiological strategies. *Pharmacol Ther*. 2022;233:108024.

doi: 10.1016/j.pharmthera.2021.108024

36. Gaillard T. Evaluation of AutoDock and AutoDock Vina on the CASF-2013 Benchmark. *J Chem Inf Model*. 2018;58(8):1697-1706.

doi: 10.1021/acs.jcim.8b00312

37. Schwartz RH. T cell anergy. *Annu Rev Immunol*. 2003;21(1):305-334.

doi: 10.1146/annurev.immunol.21.120601.141110

38. Pardoll DM. The blockade of immune checkpoints in cancer immunotherapy. *Nat Rev Cancer*. 2012;12(4):252-264.

doi: 10.1038/nrc3239

39. Wherry EJ, Kurachi M. Molecular and cellular insights into T cell exhaustion. *Nat Rev Immunol*. 2015;15(8):486-499.

doi: 10.1038/nri3862

40. Brizel DM, Schroeder T, Scher RL, *et al*. Elevated tumor lactate concentrations predict for an increased risk of metastases in head-and-neck cancer. *Int J Radiat Oncol Biol Phys*. 2001;51(2):349-353.

doi: 10.1016/s0360-3016(01)01630-3

41. Pucino V, Cucchi D, Mauro C. Lactate transporters as therapeutic targets in cancer and inflammatory diseases. *Expert Opinion on Therapeutic Targets*. 2018;22(9):735-743.

doi: 10.1080/14728222.2018.1511706

42. Pérez-Tomás R, Pérez-Guillén I. Lactate in the Tumor Microenvironment: An Essential Molecule in Cancer Progression and Treatment. *Cancers*. 2020;12(11):3244.

doi: 10.3390/cancers12113244

43. Fischer K, Hoffmann P, Voelkl S, *et al*. Inhibitory effect of tumor cell-derived lactic acid on human T cells. *Blood*. 2007;109(9):3812-3819.

doi: 10.1182/blood-2006-07-035972

44. Raychaudhuri D, Singh P, Chakraborty B, *et al*. Histone lactylation drives CD8(+) T cell metabolism and function. *Nat Immunol*. 2024;25(11):2140-2151.

doi: 10.1038/s41590-024-01985-9

45. Kaanane H, Senhaji N, Berradi H, *et al*. The influence of Interleukin-6, Interleukin-8, Interleukin-10, Interleukin-17, TNF-A, MIF, STAT3 on lung cancer risk in Moroccan population. *Cytokine*. 2022;151:155806.

doi: 10.1016/j.cyto.2022.155806

46. de la Cruz-López KG, Castro-Muñoz LJ, Reyes-Hernández DO, *et al*. Lactate in the Regulation of Tumor Microenvironment and Therapeutic Approaches. *Front Oncol*. 2019;9.

doi: 10.3389/fonc.2019.01143

47. Lin S, Wang M, Liu X, *et al*. Association of genetic polymorphisms in MIF with breast cancer risk in Chinese women. *Clin Exp Med*. 2017;17(3):395-401.

doi: 10.1007/s10238-016-0439-9

48. Zhu GQ, Tang Z, Huang R, *et al*. CD36(+) cancer-associated fibroblasts provide immunosuppressive microenvironment for hepatocellular carcinoma via secretion of macrophage migration inhibitory factor. *Cell Discov*. 2023;9(1).

doi: 10.1038/s41421-023-00529-z

49. Jia X, Xi J, Tian B, *et al*. The Tautomerase Activity of Tumor Exosomal MIF Promotes Pancreatic Cancer Progression by Modulating MDSC Differentiation. *Cancer Immunol Res*. 2023;12(1):72-90.

doi: 10.1158/2326-6066.CIR-23-0205

50. Cohen Shvefel S, Pai JA, Cao Y, *et al*. Temporal genomic analysis of homogeneous tumor models reveals key regulators of immune evasion in melanoma. *Cancer Discov*. 2024;15(3):553-577.

doi: 10.1158/2159-8290.CD-23-1422

51. Lin T, Ren Q, Zuo W, *et al*. Valproic acid exhibits anti-tumor activity selectively against EGFR/ErbB2/ErbB3-coexpressing pancreatic cancer via induction of ErbB family members-targeting microRNAs. *J Exp Clin Cancer Res*. 2019;38(1).

doi: 10.1186/s13046-019-1160-9

52. Cai Z, Lim D, Liu G, *et al*. Valproic Acid-Like Compounds Enhance and Prolong the Radiotherapy Effect on Breast Cancer by Activating and Maintaining Anti-Tumor Immune Function. *Front Immunol*. 2021;12.

doi: 10.3389/fimmu.2021.646384

53. Chavez A, Quesenberry CP, Jr., Darbinian J, *et al*. Association of Valproic Acid Use, a Potent Histone Deacetylase Inhibitor, and Melanoma Risk. *J Invest Dermatol*. 2020;140(12):2353-2358.

doi: 10.1016/j.jid.2020.04.007

54. Han W, Shi L, Ren L, *et al*. A nanomedicine approach enables co-delivery of cyclosporin A and gefitinib to potentiate the therapeutic efficacy in drug-resistant lung cancer. *Signal Transduct Target Ther*. 2018;3(1).

doi: 10.1038/s41392-018-0019-4

55. Liu H, Chai Z, Gao Y, *et al*. Ivermectin inhibits the growth of ESCC by activating the ATF4-mediated endoplasmic reticulum stress-autophagy pathway. *Acta Biochim Biophys Sin*. 2024;57(6):995-1005.

doi: 10.3724/abbs.2024210

56. Que ZJ, Yao JL, Zhou ZY, *et al*. Jinfukang inhibits lung cancer metastasis by upregulating CX3CL1 to recruit NK cells to kill CTCs. *J Ethnopharmacol*. 2021;275:114175.

doi: 10.1016/j.jep.2021.114175